# A compact, large-range interferometer for precision measurement and inertial sensing

S. J. Cooper,[1, *] A. C. Green,[1] C. Collins,[1] D. Hoyland,[1] C. C. Speake,[1] A. Freise,[1] and C. M. Mow-Lowry[1]

[1]*University of Birmingham, Birmingham, B15 2TT, UK*

(Dated: October 16, 2017)

We present a compact, fibre-coupled interferometer with high sensitivity and a large working range. We propose to use this interferometer as a readout mechanism for future inertial sensors, removing a major limiting noise source, and in precision positioning systems. The interferometer's peak sensitivity is $2 \times 10^{-14}\,\mathrm{m}/\sqrt{\mathrm{Hz}}$ at 70 Hz and $8 \times 10^{-11}\,\mathrm{m}/\sqrt{\mathrm{Hz}}$ at 10 mHz. If deployed on a GS-13 geophone, the resulting inertial sensing output will be dominated by suspension thermal noise from 50 mHz to 2 Hz.

## I. INTRODUCTION

On the 14th September 2015 the Advanced Laser Interferometer Gravitational-wave Observatory (LIGO) made the first direct detection of gravitational waves [1, 2]. To achieve the extraordinary sensitivity required for this discovery, Advanced LIGO uses a complex configuration of suspended mirrors to enhance the signal-to-noise performance of the detector. The mirrors are held at a precise operating point via closed-loop feedback systems, to ensure the light in the interferometer is resonant in the various optical cavities. In order to reduce the required feedback forces, and associated noise, all core interferometer components are placed on Internal Seismic Isolation (ISI) systems to reduce their inertial and relative motion. The ISIs employ many high-precision inertial and position sensors to reduce the transmission of ground motion [3].

The inertial sensors employed by LIGO have internal noises that are substantially higher than the suspension thermal noise limit of their proof masses [4, 5]. Using interferometers to measure the proof mass position has the potential to remove some of the existing limitations in readout and actuation noise. Other groups [6–10] have had success in improving the performance of inertial sensors using optical readout.

We present a compact interferometer based on the EUCLID and ILIAD sensors developed at Birmingham [11–13]. We achieve sufficient sensitivity to reach the suspension thermal noise of a Geotech Instruments GS-13 geophone from 80 mHz to 2 Hz, and that is approximately three orders of magnitude more sensitive than the position sensors (BOSEMs) used to provide local damping of Advanced LIGO's suspended mirrors [12, 14]. For inertial sensors, these improvements have the potential to meet future needs [15] and allow LIGO to operate in a wider variety of environmental conditions, increasing observation time. The performance of inertial sensors with improved low-frequency sensitivity is evaluated in this paper by their ability to improve the performance of the Advanced LIGO interferometers, however they have several other applications including in atom interferometers [16–18] and particle accelerators [19].

## II. SENSITIVITY REQUIREMENTS

At the LIGO detector sites the ground motion at 10 Hz is approximately 10 orders of magnitude larger than measured gravitational-wave signals. The use of complex multi-stage passive and active isolation systems attenuates input motion below other noise sources at frequencies above 10 Hz [20]. Despite this, ground motion at frequencies below 1 Hz, where active feedback provides most of the isolation, can still increase the RMS motion of the interferometer mirrors enough to prevent operation. The primary contributions to residual motion between the optics (excluding earthquakes) comes from the secondary micro-seismic peak (typically between 0.15 and 0.35 Hz) and the coupling between tilt and translation (typically below 0.1 Hz) [21].

The control band for LIGO's active inertial isolation is approximately 100 mHz to 30 Hz [22]. At low frequencies the inertial sensing output is blended with displacement sensors such that the isolated platforms are effectively locked to the ground below approximately 30 mHz. However due to the constraints of causal filtering, the inertial sensors must perform well down to 10 mHz to avoid injecting sensor-noise or tilt-coupling. Performance requirements between 1 and 10 Hz mean that the unity gain frequency must be about 30 Hz, and as such good inertial sensor performance (in both sensitivity and phase response) is needed up to 100 Hz. For these reasons, to be of interest for Advanced LIGO (and other gravitational-wave detectors) any new inertial sensor should have sensitivity at least equal to state-of-the-art inertial sensors between 10 mHz and 100 Hz.

Further improvements to the interferometer's performance can be made by increasing the sensitivity of the BOSEM displacement sensors placed on LIGO's quadruple suspensions [23]. Due to the noise of the BOSEMs, local feedback forces can only be applied to the uppermost suspended mass, and even then the control filters have strict requirements imposed by the need to prevent sensor noise from spoiling the detector sensitivity at 10 Hz [14]. Interferometric displacement sensors would allow

---

for improved damping at the uppermost mass, and possibly allow local-damping on lower stages, reducing both vibration transmission and settling time. To apply significant damping using a sensor at the second stage, the noise of the sensor at 10 Hz should be reduced by a factor of order $10^2$, approximately matching the increase in transmissibility [24].



FIG. 1: The optical layout of HoQI. Orthogonal polarisation states are used to track the length difference between Lx and Ly over multiple optical fringes. The input beam is split at polarising beamsplitter PBS2 and interferometrically recombined at PBS1 and PBS3, producing signals proportional to the sine, cosine, and minus cosine of the optical phase difference. Grey arrows indicate the direction of propagation.

## III. READOUT SCHEME AND OPTICAL LAYOUT

A standard two-beam interferometer has a narrow operating range, typically less than a quarter of a wavelength of total path-length difference. To increase both the dynamic range and the operating range, without using actuators or modulation schemes, we employ a Homodyne Quadrature Interferometer (HoQI) that can measure two nearly orthogonal quadratures of the interferometer output. In this case, we use a Mach-Zender interferometer with two independent recombination beamsplitters. A polarisation scheme is employed to generate the required differential phase shift [25].

Compared with EUCLID, the optical path, shown schematically in Fig.1, is significantly simpler in order to reduce birefringence noise and reduce stray light effects. One of the elements removed is the tilt compensation system [26]. This reduces the number of birefringent elements, but at the cost of larger susceptibility to tilt. To reduce frequency noise, we use a narrow-linewidth 1064 nm solid-state Innolight Mephisto 500NE laser (1 kHz linewidth for 0.1 s averaging period) in place of the VCSEL diode laser, and we carefully match the arm lengths. Assuming the target mirror remains aligned (or a suitable corner cube is used), the operating range of HoQI is only limited by the fringe visibility degradation due to spot-size changes, and it is at least 10 mm for this configuration.

The laser light is fibre-coupled to the interferometer by a 2 m single-mode polarisation maintaining fibre with an input power of 10 mW. The first Polarising BeamSplitter, PBS1, ensures there is a clean input polarisation state. PBS2 splits the input beam into two orthogonally polarised beams, one for each arm. These beams are recombined at PBS2 and co-propagate without interfering. The beam is divided, again without interference, at the Non-Polarising BeamSplitter (NPBS). The quarter-wave plate before PBS3 then adds an additional phase shift of 90 degrees to the light from one of the arms such that when the beams interfere at PBS1 and PBS3, the resulting intensity fluctuations are 90 degrees out of phase. The power measured on the photodiodes is given by the following equations,
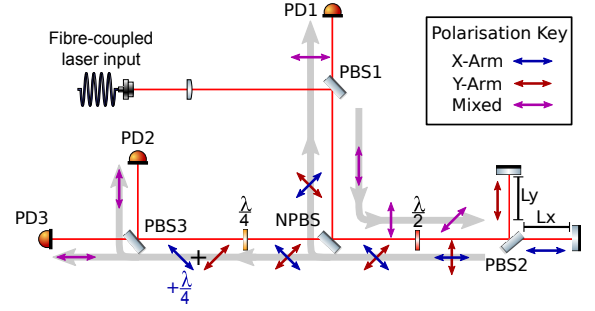
$$\text{PD1} = \frac{P_{in}}{8}(1 + a\sin(\phi_{opt})), \tag{1}$$

$$\text{PD2} = \frac{P_{in}}{8}(1 + a\cos(\phi_{opt})), \tag{2}$$

$$\text{PD3} = \frac{P_{in}}{8}(1 - a\cos(\phi_{opt})), \tag{3}$$

$$\text{PD1} - \text{PD2} = \frac{\sqrt{2}aP_{in}}{8}\sin(\phi - \frac{\pi}{4}), \tag{4}$$

$$\text{PD1} - \text{PD3} = \frac{\sqrt{2}aP_{in}}{8}\sin(\phi + \frac{\pi}{4}), \tag{5}$$

where $P_{in}$ represents the input power, a is the fringe visibility and $\phi_{opt}$ represents the differential optical phase and is defined as $\phi_{opt} = \frac{4\pi(L_x - L_y)}{\lambda}$. Equations 4 and 5 show how these signals can be combined to provide substantial common-mode rejection of laser intensity noise by reducing the dependence on both the input power and the fringe visibility.

Unwrapping the 4-quadrant arctangent of equations 4 and 5 returns the optical phase. To achieve high resolution, each photodiode signal is digitised with a high dynamic range, 18-bit ADC and the arctangent is performed using a cordic engine implemented on an FPGA. The analogue front-end and digital processing use an electronics module developed for the EUCLID and ILIAD interferometers [11], which have exceptionally low input-referred noise at low-frequencies and a proven signal processing chain. The displacement-equivalent noise of the readout electronics is shown in Fig.3, and it is what enables the high precision reported here.
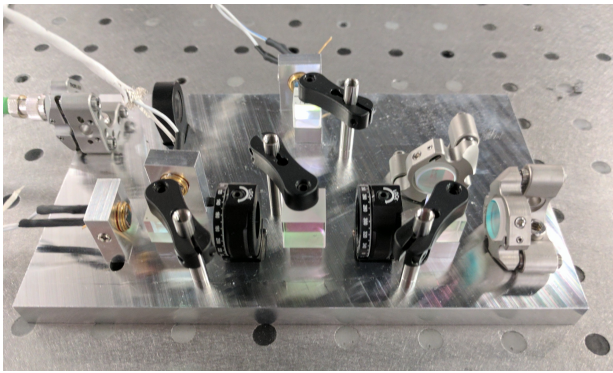
FIG. 2: The prototype version of HoQI, the base plate is $170 \times 100\,\mathrm{mm}$ with $10\,\mathrm{mm}$ gaps between components.

## IV. RESULTS

To investigate the sensitivity limits of HoQI we reduced optical and mechanical noise where possible. The largest anticipated sources of noise were: mechanical vibration, thermal expansion and gradients, birefringence noise, frequency noise, and electronic noise. All optics were rigidly mounted close together on an aluminium baseplate with a relatively large thermal mass, seen in Fig. 2, resulting in large common-mode rejection of mechanical noise and reducing thermal gradients.

Birefringence fluctuations between the non-polarising beamsplitter and the recombination polarising beam-splitters are indistinguishable from arm-length changes. Since the beams are well aligned and co-propagate, the dominant effect is expected to come from quarter-wave plate, and a high the-quality zero-order plate was used to reduce this. Alignment fluctuations on the photodi-odes cause uncorrelated fluctuations in the photocurrent due to inhomogeneities in the quantum efficiency. The single-mode fibre strips away pointing fluctuations, and the output mode is mechanically fixed to the baseplate by the fibre output collimator.

Frequency noise coupling was measured and minimised by modulating the laser frequency and adjusting the macroscopic arm-length difference to minimise the coupling to differential optical phase. The length was precisely tuned using the alignment screws on the 'end' mirrors, with a resolution of a few microns, but the coupling was much larger than predicted. This is attributed to scattered light interferometers within the baseplate. The residual coupling can be quantified by an effective arm-length mismatch of $0.7\,\mathrm{mm}$. Assuming laser frequency fluctuations of $10^4 \times [\frac{1}{f}]\,\mathrm{Hz}/\sqrt{\mathrm{Hz}}$, we predict the red curve shown in Fig. 3.

The electronic noise (the black curve in 3) is measured by replacing the photodiode inputs with a constant current using a resistor connected to a bias voltage. The resistor values are such that the 3 input currents simulate a specific optical phase for the three photodiodes.

The baseplate was placed on rubber 'feet' on an optical

bench and sampled at $20\,\mathrm{kHz}$ over a 10 hour period. Fig.3 shows the amplitude spectral density of the measurement over a ten minute segment of this data. The interferometer reaches a peak sensitivity of $2 \times 10^{-14}\,\mathrm{m}/\sqrt{\mathrm{Hz}}$ at $70\,\mathrm{Hz}$. At $10\,\mathrm{mHz}$ a sensitivity of $8 \times 10^{-11}\,\mathrm{m}/\sqrt{\mathrm{Hz}}$ is achieved.
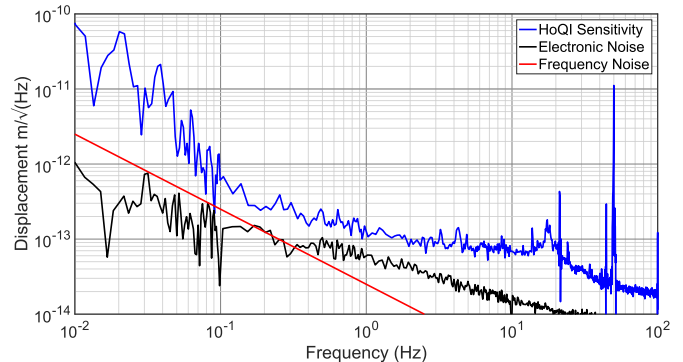


FIG. 3: Sensitivity of the fibre-coupled prototype HoQI showing the interferometer signal (blue), the measured readout noise (black), and an estimate of the frequency noise that couples into the interferometer (red)

The total sensitivity is probably limited by electronic noise at frequencies near $0.5\,\mathrm{Hz}$. Below this, the limiting factor is assumed to be a combination of air currents, temperature fluctuations, and frequency noise. Above $1\,\mathrm{Hz}$, the sources of noise are less well understood except for the peak near $18\,\mathrm{Hz}$, that is caused by mechanical vibration of the optical table, and the large peak at $50\,\mathrm{Hz}$, caused by pickup in the unshielded photodiode cables.

Fig.4 compares the sensitivity of HoQI with the Capacitive Position Sensors (CPS), which are employed on the first stage of LIGO's Internal Seismic Isolation system (ISI). In the frequency band of interest they offer 250 times lower noise at $100\,\mathrm{mHz}$ and 1000 times lower noise at $10\,\mathrm{Hz}$. When compared with the BOSEMs, the improvement is more substantial: HoQI has a factor of 500 lower noise at $100\,\mathrm{mHz}$ and 1000 times lower noise at $10\,\mathrm{Hz}$.

In order to compare HoQI's readout noise with existing inertial sensors, we multiply the interferometer sensitivity curve by the inertial-sensing transfer function of both a GS-13 and a Watt's linkage similar to those employed at the Virgo gravitational-wave detector [27]. The result of this is shown in Fig.5. This readout-noise is then summed in quadrature with the estimated suspension thermal noise for each sensor. The GS-13 is assumed to have a $5\,\mathrm{kg}$ proof-mass, a resonant frequency of $1\,\mathrm{Hz}$, and a quality factor of 40. The Watt's linkage, with its low mechanical-dissipation and resonant frequency, has lower thermal noise (everywhere) and lower readout noise below $1\,\mathrm{Hz}$. For the suspension thermal noise calculation we assume a proof-mass of $1\,\mathrm{kg}$, a resonant frequency of $0.3\,\mathrm{Hz}$, and a (structurally-damped) quality factor of 100.

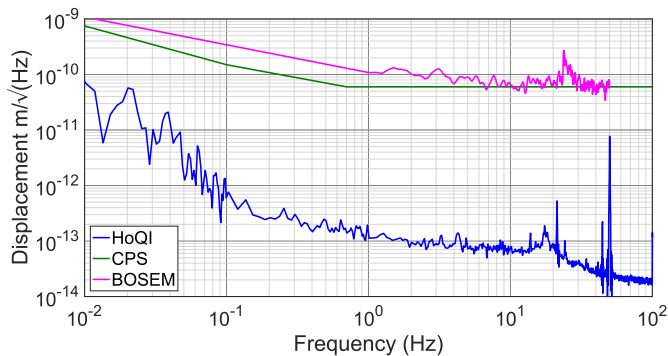The noise projections are compared with the self-noise

FIG. 4: HoQI compared with position sensors used at LIGO showing the 0.25 mm range Capacitive Position Sensor (CPS, green), the Birmingham Optical Sensor and Electro-Magnetic actuator (BOSEM, magenta), and HoQI (blue). The CPS and low-frequency BOSEM curves are stick-figure fits to noise spectra from multiple devices.
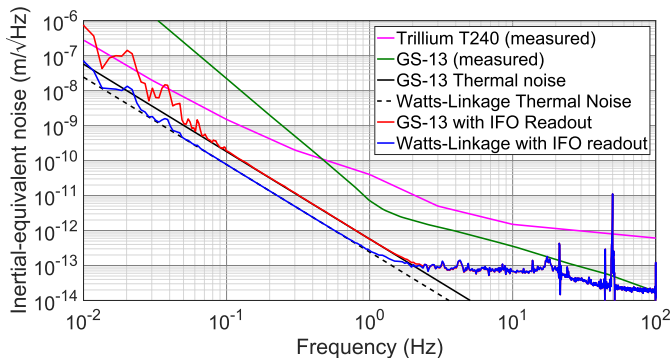


FIG. 5: The sensitivity curve of HoQI projected onto a GS-13 (red) and a Watt's linkage (blue) is compared with a GS-13 using conventional readout (green), and a Trillium T-240 force-feedback seismometer (magenta). The (calculated) suspension thermal noise of the GS-13 with a structural Q of 40 (black) [28] and Watt's linkage with a structural Q of 100 (dashed black) is also shown.

floors of the GS-13 (using it's conventional coil-magnet readout) and a Trillium T240, both as measured at LIGO. We find that the inertial sensor output would be limited by the suspension thermal noise of the GS-13 from 0.1 to 2 Hz and from 80 mHz to 1 Hz for the Watt's linkage. Despite the thermal noise limitation, using HoQI to interrogate a GS-13 could increase the sensitivity by a factor of 100 at 100 mHz and would improve it at all frequencies up to 100 Hz.

## V.  CONCLUSION

We have presented a new compact interferometer that employs a homodyne phasemeter, HoQI. This combines an existing architecture with a low-noise laser and readout system to achieve excellent noise performance from 10 mHz to 100 Hz. The sensitivity is substantially better than existing displacement sensors at LIGO, sufficient to improve the performance of suspension damping systems. If used as part of an inertial sensor using existing mechanics, it could reduce the self-noise across a wide range of frequencies, down to the suspension thermal noise of the mechanical springs.

## ACKNOWLEDGMENTS

[1] B. P. Abbott, R. Abbott, T. D. Abbott, M. R. Abernathy, F. Acernese, K. Ackley, C. Adams, T. Adams, P. Addesso, R. X. Adhikari, et al. (LIGO Scientific Collaboration and Virgo Collaboration), Phys. Rev. Lett. **116**, 061102 (2016), URL http://link.aps.org/doi/10.1103/PhysRevLett.116.061102.

[2] B. Abbott, R. Abbott, T. Abbott, M. Abernathy, F. Acernese, K. Ackley, C. Adams, T. Adams, P. Addesso, R. Adhikari, et al., Physical Review Letters **116**, 241103 (2016).

[3] F. Matichard, B. Lantz, K. Mason, R. Mittleman, B. Abbott, S. Abbott, E. Allwine, S. Barnum, J. Birch, S. Biscans, et al., Precision Engineering **40**, 273 (2015).

[4] P. R. Saulson, Phys. Rev. D **42**, 2437 (1990), URL https://link.aps.org/doi/10.1103/PhysRevD.42.2437.

[5] A. Barzilai, T. VanZandt, and T. Kenny, Review of Scientific Instruments **69**, 2767 (1998), URL http://dx.doi.org/10.1063/1.1149013.

[6] M. A. Zumberge, J. Berger, M. A. Dzieciuch, and R. L. Parker, Appl. Opt. **43**, 771 (2004).

[7] M. Zumberge, J. Berger, J. Otero, and E. Wielandt, Bulletin of the Seismological Society of America **100**, 598 (2010), URL http://www.bssaonline.org/content/100/2/598.abstract.

[8] J. Watchi, B. Ding, F. Matichard, and C. Collette (2016).

[9] T. B. Arp, C. A. Hagedorn, S. Schlamminger, and J. H. Gundlach, Review of Scientific Instruments **84**, 095007 (2013), URL http://dx.doi.org/10.1063/1.4821653.

[10] K. Venkateswara, C. A. Hagedorn, M. D. Turner, T. Arp, and J. H. Gundlach, Review of Scientific Instruments

**85**, 015005 (2014), URL http://dx.doi.org/10.1063/1.4862816.

[11] C. C. Speake and S. M. Aston, Classical and Quantum Gravity **22**, S269 (2005), URL http://stacks.iop.org/0264-9381/22/i=10/a=019.

[12] S. Aston, Ph.D. thesis, Unviersity of Birmingham (2011), URL http://etheses.bham.ac.uk/1665/.

[13] F. E. P. Arellano, H. Panjwani, L. Carbone, and C. C. Speake, Review of Scientific Instruments **84**, 043101 (2013), URL http://dx.doi.org/10.1063/1.4795549.

[14] K. A. Strain and B. N. Shapiro, Review of Scientific Instruments **83**, 044501 (2012), URL http://dx.doi.org/10.1063/1.4704459.

[15] LIGO Scientific Collaboration (2015), *LIGO Voyager Instrument Science White Paper*, URL https://dcc.ligo.org/public/0113/T1400316/004/T1400316-v5.pdf.

[16] A. Miffre, M. Jacquey, M. Büchner, G. Trénec, and J. Vigué, Applied Physics B **84**, 617 (2006), ISSN 1432-0649, URL http://dx.doi.org/10.1007/s00340-006-2377-9.

[17] M.-K. Zhou, Z.-K. Hu, X.-C. Duan, B.-L. Sun, L.-L. Chen, Q.-Z. Zhang, and J. Luo, Phys. Rev. A **86**, 043630 (2012), URL http://link.aps.org/doi/10.1103/PhysRevA.86.043630.

[18] M.-K. Zhou, X. Xiong, L.-L. Chen, J.-F. Cui, X.-C. Duan, and Z.-K. Hu, Review of Scientific Instruments **86**, 046108 (2015), URL http://dx.doi.org/10.1063/1.4919292.

[19] C. Collette, S. Janssens, P. Fernandez-Carmona, K. Artoos, M. Guinchard, C. Hauviller, and A. Preumont, Bulletin of the Seismological Society of America **102**, 1289 (2012), URL http://www.bssaonline.org/content/102/4/1289.abstract.

[20] J. Aasi, B. P. Abbott, R. Abbott, T. Abbott, M. R. Abernathy, K. Ackley, C. Adams, T. Adams, P. Addesso, R. X. Adhikari, et al., Classical and Quantum Gravity **32**, 074001 (2015), URL http://stacks.iop.org/0264-9381/32/i=7/a=074001.

[21] B. Lantz, R. Schofield, B. O‚ÄôReilly, D. E. Clark, and D. DeBra, Bulletin of the Seismological Society of America **99**, 980 (2009), URL http://www.bssaonline.org/content/99/2B/980.abstract.

[22] F. Matichard, B. Lantz, R. Mittleman, K. Mason, J. Kissel, B. Abbott, S. Biscans, J. McIver, R. Abbott, S. Abbott, et al., Classical and Quantum Gravity **32**, 185003 (2015), URL http://stacks.iop.org/0264-9381/32/i=18/a=185003.

[23] L. Carbone, S. M. Aston, R. M. Cutler, A. Freise, J. Greenhalgh, J. Heefner, D. Hoyland, N. A. Lockerbie, D. Lodhia, N. A. Robertson, et al., Classical and Quantum Gravity **29**, 115005 (2012), URL http://stacks.iop.org/0264-9381/29/i=11/a=115005.

[24] B. Shapiro, Private Communication (2017).

[25] G. M. B. Bouricius and S. F. Clifford, Review of Scientific Instruments **41**, 1800 (1970), URL http://dx.doi.org/10.1063/1.1684414.

[26] F. E. P. na Arellano and C. C. Speake, Appl. Opt. **50**, 981 (2011), URL http://ao.osa.org/abstract.cfm?URI=ao-50-7-981.

[27] F. Barone, G. Giordano, F. Acernese, and R. Romano, Nuclear Instruments and Methods in Physics Research Section A: Accelerators, Spectrometers, Detectors and Associated Equipment **824**, 187 (2016), URL http://www.sciencedirect.com/science/article/pii/S0168900215013777.

[28] D. Clark and B. Lantz, Tech. Rep. (2009), URL https://dcc.ligo.org/LIGO-T0900089/public.